aerospace

MDPI

Article

A Rapid Modeling Method for Airborne FSS Radomes Based on Dynamic Customizable Primitives

Cunai Qiu [1], Shen Li [1,*], Wenwu Zhang [1,2], Liwei Song [1], Xiang Li [1], Zhongen Yan [1], Yue Chen [1] and Saisai Suo [1]

[1] State Key Laboratory of Electromechanical Integrated Manufacturing of High-Performance Electronic Equipments, Xidian University, Xi'an 710071, China; 22041212834@stu.xidian.edu.cn (C.Q.); 23043110475@stu.xidian.edu.cn (W.Z.); lwsong@xidian.edu.cn (L.S.); 22041212835@stu.xidian.edu.cn (X.L.); 23041212800@stu.xidian.edu.cn (Z.Y.); 23041212706@stu.xidian.edu.cn (Y.C.); 22041212808@stu.xidian.edu.cn (S.S.)

[2] Avic Research Institute for Special Structures of Aeronautical Composites, Ji'nan 250023, China

* Correspondence: sli@xidian.edu.cn; Tel.: +86-1351-916-1841

Abstract: The digital model of airborne frequency selective surface radomes (AFSSRs) is the basis of design, simulation analysis, manufacturing, and other related research on AFSSRs. This paper proposes a rapid modeling method for AFSSRs based on dynamic customizable primitives. Firstly, a layered digital model construction scheme for AFSSRs is presented based on the typical radome wall structure. Then, according to the characteristics of various surface configurations and the complex wireframe information of AFSSRs, the dynamic primitives are raised to express the boundary and contour information of all kinds of radomes. Focusing on the undevelopable characteristics of the aerodynamic shape surface of the AFSSR, the arrangement solution and mapping method for frequency-selective elements on undevelopable surfaces are proposed. Furthermore, the implementation logic of this method for the creation of each layer model and the assembly of the whole machine model is introduced. Finally, a rapid modeling system (RMS) is established based on this method, enabling the automated creation of digital models of AFSSRs. Utilizing this system resulted in modeling time savings ranging from 20% to 97.5% compared to traditional methods, which verifies the feasibility and effectiveness of this method.

Keywords: airborne frequency selective surface radome (AFSSR); primitives; rapid modeling

check for updates

Citation: Qiu, C.; Li, S.; Zhang, W.; Song, L.; Li, X.; Yan, Z.; Chen, Y.; Suo, S. A Rapid Modeling Method for Airborne FSS Radomes Based on Dynamic Customizable Primitives. *Aerospace* **2024**, *11*, 505. https://doi.org/10.3390/aerospace11070505

Academic Editor: Yan (Rockee) Zhang

Received: 15 April 2024
Revised: 31 May 2024
Accepted: 5 June 2024
Published: 23 June 2024

Copyright: © 2024 by the authors. Licensee MDPI, Basel, Switzerland. This article is an open access article distributed under the terms and conditions of the Creative Commons Attribution (CC BY) license (https://creativecommons.org/licenses/by/4.0/).

1. Introduction

Modern war is essentially a battle for information control rights, electromagnetic (EM) control rights, and air control rights. Aviation weapons and equipment play a huge role in modern war and have become a crucial factor affecting the outcome of war. As the goggle of the airborne radar antenna, the airborne radome is a key structure to improve the aerodynamic shape of the airborne carrier and protect the radar antenna from working normally in extreme environments. It is widely used in typical airborne weapons platforms such as fourth-generation or fifth-generation fighters, unmanned aerial vehicles, and tactical missiles [1–4]. At the same time, to improve the penetration ability and survivability of our airborne weapon platforms and avoid the enemy's reconnaissance, detection, and interference, frequency selective surfaces (FSSs) technology is usually used to present the stealth performance of the airborne radome in a specific frequency band [5–7]. An FSS refers to an aperture periodically arranged on the surface of a conductive metal or a metal patch arranged on the surface of a dielectric, which is essentially a spatial filter. Loading FSSs onto the wall of the airborne radome will make the airborne radome have frequency selectivity, which can effectively improve the stealth ability of airborne weapon platforms [8–11].

Due to the important application value of airborne frequency selective surface radomes (AFSSRs) in the military field, the related technology of AFSSRs has become a research

hotspot at home and abroad. Choi et al. [12] designed a low-observable composite sandwich structure radome composed of E-glass/epoxy or aramid/epoxy composite faces, polymethacrylimide foam core, and an FSS. The radome has good EM transmission characteristics in the X-band, and its mechanical properties are better than those of conventional composite radomes. Narayan et al. [13] presented a swastika-shaped novel metamaterial (MTM) element and designed an airborne hemispherical radome with an MTM-FSS structure based on this element. The radome has superior EM performance in the frequency range of 8.5–10.3 GHz, with high transmission efficiency (~0.30 dB insertion loss) and minimal boresight error (~4 mrad) in the entire beam steering range. Liu et al. [14] proposed an optimal design method for FSS radomes. This method uses the pixel-overlap technique to improve the manufacturability of FSS layers and uses the binary particle swarm optimization algorithm to obtain the structural parameters of the FSS radome. A FSS radome is designed and simulated by using the optimized FSS element. When the incident angle reaches 50°, the transmission coefficient stays above −2 dB in the pass band and below −10 dB in the stop band, indicating the method's feasibility. Rafieipour et al. [15] put forward a hybrid stacking sequence design of composites by using the complex proportional assessment method and considering the mechanical properties, EM performance, and moisture resistance of the experimental specimens. Combined with a genetic algorithm, an embedded FSS is designed. Compared with the traditional FSS performance, the design can not only achieve maximum transmission at the resonance frequency but also enhance transmission loss outside of the desired frequency band. However, the design and simulation of the FSS and the airborne radome loaded with the FSS under different conditions are generally based on the ideal plane model or flat plate sample, and the AFSSRs often have a specific aerodynamic shape (such as rotary type, duckbill type, prismatic shape, etc.) [16,17]. The EM performance of the airborne FSS radome designed based on ideal conditions often fails to meet the initial design specifications in actual service.

Wang et al. [18] proposed a variable-thickness streamlined radome wall structure with graded dielectric multilayered walls for airborne applications. Vinisha et al. [19] designed a five-layer symmetrically cascaded radome wall structure with a dielectric constant gradually increasing from the outer layer to the inner layer. Xu has performed in-depth research on structural optimization, profile design, and EM performance of variable-thickness radomes [20,21], and the EM performance of inhomogeneous radomes [16,22]. Nóbregaa et al. [23] designed a compact, dual-polarized FSS structure with a high-frequency compression coefficient (66.08%) and excellent angular stability by racializing the Sierpinski geometric structure. Inspired by fractal geometries, Murugasamy et al. [24] presented a four-legged loaded loop element of third-order iteration and applied it to a 2.5-D FSS. Yang et al. [25] cascaded the double-layer FSS and dielectric ceramic coating to form a radar absorber structure. One layer of FSS consisted of square and circular metal period arrays that couple with each other, and another consisted of period arrays with square patches. The structure has distinguished microwave-absorbing properties. At the structural level, AFSSRs are developing into complex forms such as multilayer dielectric and metal stacking of the wall structure, variable thickness or inhomogeneity of the aerodynamic contour, fractal and multi-dimensional FSS elements, and cascades of multilayer FSS [26,27]. Nevertheless, the existing computer-aided design or engineering (CAD/CAE) model creation methods of FSS radomes (such as conventional manual modeling methods, HFSS-MATLAB, combined modeling methods, etc.) and related EM simulation software (HFSS, CST, FEKO, etc.) make it difficult to create models for diversified and complex structural design requirements.

Parametric modeling technology is a typical computer-aided design method that is widely used in aerospace, ships, electronics, and other fields [28,29]. Chen et al. [30] proposed an isogeometric size optimization design method based on parameterized volume parametric models. This method takes size parameters as high-level parameter input and realizes the integration of the design process, including geometric modeling, performance analysis, and structural optimization. It can be applied to the

integrated optimization design of complex mechanical structures. Zheng et al. [31] applied parametric modeling technology to propeller design and proposed an improved parametric model called iPM4MP to construct CAD models of marine propellers. The iPM4MP can build a valid CAD geometry and maintain the generality of the shape while decreasing the number of free variables. It has certain advantages in outlining the shape of the blade tip. Tang et al. [32] presented a decision-support method for multi-parameter editing of parametric CAD models. The method supports decision-making in multi-parameter model editing by calculating the allowable parameter range, assists users in realizing model editing, and ensures the solvability of the geometric constraint system. However, AFSSRs do not always have a regular shape structure, and they have various surface configurations, complex wire-frame information, and numerous structural parameters with weak correlation. It is difficult to carry out parametric design through basic features or sketches. In the meantime, the locations of FSS elements on the FSS are different, and it is hard to control them uniformly by parameters. Therefore, the parametric modeling technology is not suitable for the digital modeling of AFSSRs.

The digital model of AFSSs is the research foundation for the development and design, simulation and analysis, manufacturing, testing and verification, maintenance, and modification of AFSSs. Nonetheless, there is currently no systematic method or mature software available that can provide a solution for the digital modeling of AFSSRs, which limits the research of related technologies. Based on the research mentioned above challenges and technical obstacles in the digital modeling of AFSSRs, this paper proposes a rapid modeling method for AFSSRs based on dynamic customizable primitives, aiming to realize the customization, precision, automation, and rapid creation of the digital model of AFSSRs.

This paper is structured as follows: Section 1 discusses the application background of AFSSRs and the shortcomings of existing research on the digital model of AFSSRs. Section 2 outlines the underlying support, logic implementation, and design goals of our proposed method and presents its core idea. Section 3 introduces the modeling layered scheme of the solid-core and A-sandwich wall structures of AFSSRs. Then, according to the characteristics of various surface configurations and the complex wireframe information of AFSSRs, the dynamic primitives are raised to express the boundary and contour information of all kinds of radomes. Focusing on the undevelopable characteristics of the aerodynamic shape surface of the AFSSR, the arrangement solution and mapping method for FSS elements on undevelopable surfaces are proposed. Finally, the implementation logic of this method for the creation of each layer model and the assembly of the whole machine model is introduced. Section 4 established a rapid modeling system (RMS) for AFSSRs based on this method. Meanwhile, the modeling effect and efficiency of the RMS are demonstrated and compared, which verifies the feasibility and effectiveness of this method. Lastly, conclusions are presented in Section 5.

2. Design Idea

The rapid modeling method for AFSSRs based on dynamic customizable primitives utilizes the primitives' expression files (PEFs) of the AFSSR's contour curves and the FSS element as the underlying support. The modeling functions of the dielectric layers and FSS layers, along with the assembly function of the whole machine model, serve as the logical implementation to achieve the application goal of creating a digital model of the AFSSR. The underlying support PEF adopts a file format that expresses the basic geometric elements and structural parameters of the contour curves and FSS elements in the AFSSR's framework model. During the model creation process, model customization is achieved by adjusting the PEF framework, while model precision is ensured through adjustments to the PEF's modeling parameters. The logical implementation is based on commercial CAD software application programming interfaces (APIs), incorporating rules for primitive expression, arrangement solution, and mapping methods for FSS elements on undevelopable surfaces, manual modeling approaches, manual modeling knowledge

encapsulation into modeling functions of the dielectric layers and FSS layers, and assembly functions of the whole machine model.

The design idea of this method is shown in Figure 1, which starts with the structural designers identifying the influencing factors for the EM design of the AFSSR. These factors include the EM indicators of antennas inside the radome and itself, environmental parameters during service, material parameters, processing indexes, strength requirements, and stiffness requirements [33–36]. Subsequently, based on these factors, the structural form and modeling parameters of the digital model for the AFSSR are determined, including the aerodynamic shape and dimension parameters of the AFSSR's body, the structure of the AFSSR's wall, the type and structural parameters of the FSS element, the periodic structure of the FSS, and the number and position of FSS loads. By analyzing the aerodynamic shape and integrating it with the dimensional parameters of the AFSSR's body, the PEF of the AFSSR's contour curves can be generated. Through analysis of the basic geometric elements of the FSS element and combining them with the structural parameters of the FSS element, the PEF of the FSS element can be created. Additionally, considering the structure of AFSSR's wall and the number and position of FSS loads, a layered digital model construction scheme is established. According to the layered scheme of the AFSSR, the number of layers of the dielectric layers and the FSS layers in the digital model of the AFSSR and their interrelationships are determined. The dielectric layers or the FSS layers models are created by reading the corresponding PEF and calling the modeling functions of the dielectric layers or the FSS layers. Finally, by invoking the assembly function of the whole machine model and importing the sub-models of each layer for automated assembly, the integrated AFSSR model is generated, thereby achieving the customization, precision, automation, and rapidity creation of the digital model of the AFSSR.

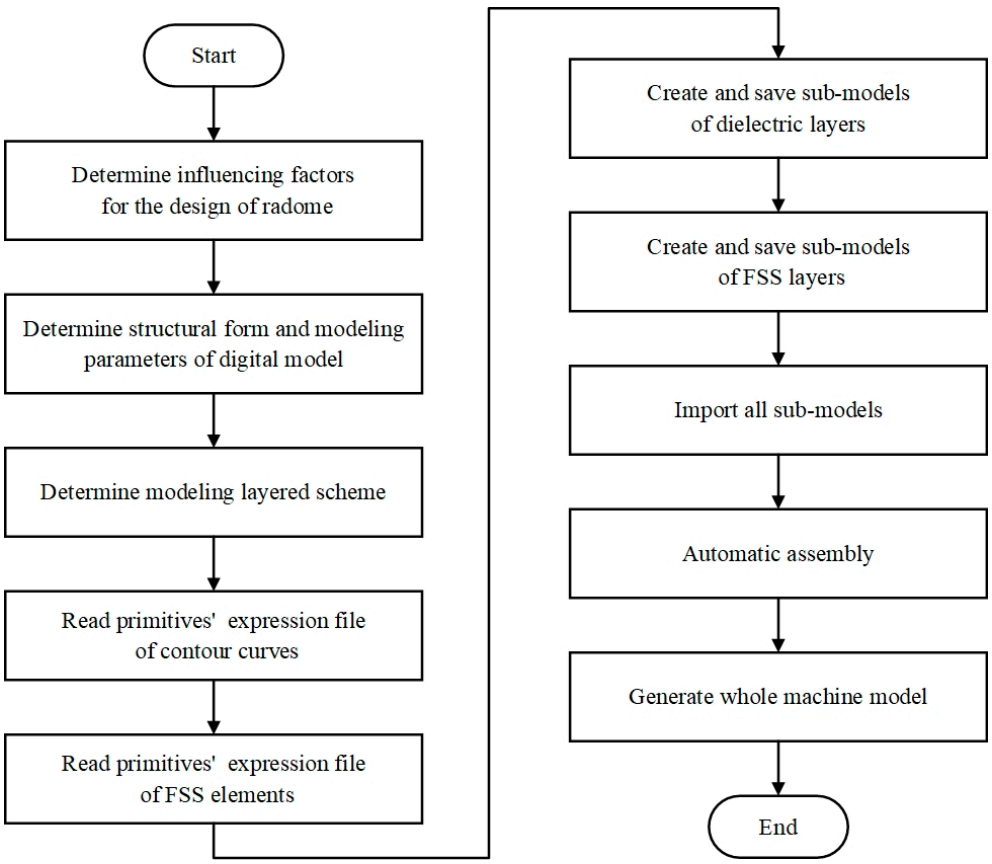


Figure 1. The design idea of the rapid modeling method for AFSSRs based on dynamic customizable primitives.

3. Methodology

3.1. The Modeling Layered Scheme

In the traditional radome structure design, the wall design of the solid-core structure is mainly used, such as the thin wall structure and the half-wave wall structure. The wall thickness of the thin wall structure is generally less than 1/10~1/20 of the wavelength, while the wall thickness of the half-wave wall structure is

$$d = \frac{\lambda}{2\sqrt{\varepsilon - \sin^2\alpha}} \quad (1)$$

where λ is the wavelength, ε is the relative permittivity of the dielectric material, and α is the incident angle [36].

To meet higher requirements for EM performance and mechanical properties, current AFSSRs often adopt a sandwich structure design for the radome wall, with common forms including A-sandwich, B-sandwich, and C-sandwich structures. The A-sandwich structure consists of two layers of high-density skin and a low-density intermediate core layer, predominantly utilized for nose cone radomes or streamlined radomes on small aircraft. In contrast, the B-sandwich structure bears a resemblance to the A-sandwich configuration, differing in that the material properties of each layer are inverted. It comprises two layers of low-density skin and a single layer of high-density intermediate core material, commonly applied for protective radomes in small multi-band anti-interference equipment as well as in millimeter-wave and sub-millimeter-wave radomes. As for the C-sandwich structure, it comprises two layers of an A-sandwich structure and is typically deployed in radomes necessitating both high-strength and high-frequency bandwidth. Generally, skin materials are selected from fiber-reinforced resin matrix composites and reinforced ceramic matrix composites. The sandwich structures commonly feature materials such as honeycomb or foam, including Nomex paper honeycomb, phenolic resin, polyurethane foam, and polystyrene foam, among others [37–39].

For AFSSRs with solid-core wall structures, the FSS can be loaded on the inner side, outer side, or middle of the solid-core wall. Figure 2a illustrates the wall structure loaded with one layer of an FSS and two layers, respectively. Meanwhile, for AFSSRs with an A-sandwich wall structure, the FSS is typically placed at the skin-core junction or within the low-density layer [36,40]. Figure 2b demonstrates the wall structure loaded with one, two, three, and four layers of an FSS, respectively. Based on the typical wall structure forms of AFSSRs and the number and position of FSS loads, a layered digital model construction scheme for AFSSRs is proposed. The AFSSRs are layered according to the division of the FSS layer and the medium layer. The number of layers and the position relationship between the medium layer and the FSS layer of the AFSSR are the modeling layered scheme of the digital model. Each layer model is established in turn and then assembled according to the positional relationship of each layer. Eventually, the whole machine model of the AFSSR model can be obtained.

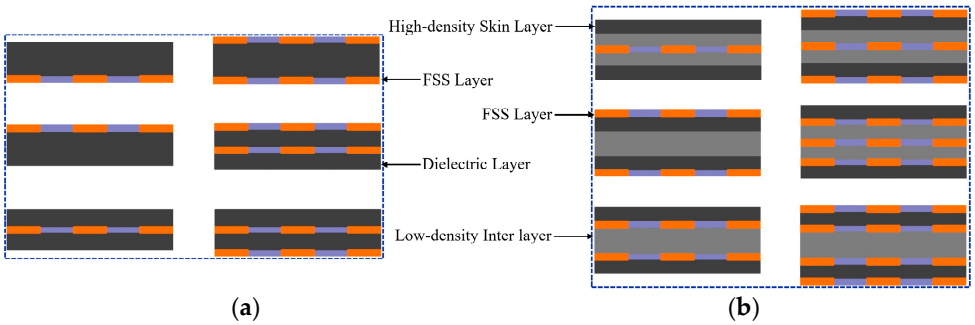


Figure 2. The modeling layered scheme for typical radome wall structures: (**a**) a modeling layered scheme for the solid-core AFSSR wall structure; (**b**) a modeling layered scheme for the A-sandwich AFSSR wall structure.

3.2. Expression Rules of Primitives

The wireframe model is a direct extension from the two-dimensional engineering drawings of geometric structures to three-dimensional space, composed of spatial points, lines, and curves, which represent the boundaries and contours of spatial geometric structures by transforming 2D plane lines and curves into 3D space lines and curves. In this paper, the basic geometric elements such as spatial points, lines, and curves are dynamically customized as primitives and combined with the modeling rules of commercial CAD software and the structure forms of AFSSRs. Considering the various surface configurations and complex wireframe information of AFSSRs' digital model, different geometric elements modeling semantics are raised to represent the boundaries and contours of AFSSRs, namely the expression rules of primitives. The expression rules of different primitives are detailed below.

- Point primitive

$$POINT = \{ID, X, Y, Z\}, \tag{2}$$

where *ID* represents the modeling identifier of the point primitive, and X, Y, and Z are the x coordinate, y coordinate, and z coordinate of the point primitive modeling, respectively.

- Line primitive

$$LINE = \{ID, X_{Start},\ Y_{Start}, Z_{Start}, X_{End}, Y_{End}, Z_{End}\}, \tag{3}$$

where *ID* represents the modeling identifier of the line primitive, and X_{Start}, Y_{Start}, and Z_{Start} are the x-coordinate, y-coordinate, and z-coordinate of the starting point of the line primitive modeling, respectively, and X_{End}, Y_{End}, and Z_{End} are the x-coordinate, y-coordinate, and z-coordinate of the ending point of the line primitive modeling, respectively.

- Circle primitive

$$CIRCLE = \{ID, X_{Center}, Y_{Center}, Z_{Center},\ iRadius,\ iStartParam,\ iEndParam\}, \tag{4}$$

where *ID* represents the modeling identifier of the circle primitive, and X_{Center}, Y_{Center}, and Z_{Center} are the x-coordinate, y-coordinate, and z-coordinate of the center of the circle primitive modeling, respectively, $iRadius$ is the modeling radius of the circle primitive, $iStartParam$ denotes the starting point parameter of the circle primitive modeling, $iEndParam$ denotes the ending point parameter of the circle primitive modeling, and where $iStartParam$ and $iEndParam$ are within the range of [0, 1].

- Ellipse primitive

$$ELLIPSE = \begin{Bmatrix} ID, X_{Center}, Y_{Center}, Z_{Center}, X_{Major}, Y_{Major}, Z_{Major}, \\ iMajorRadius, iMinorRadius, iStartParam, iEndParam \end{Bmatrix}, \tag{5}$$

where *ID* represents the modeling identifier of the ellipse primitive, and X_{Center}, Y_{Center}, and Z_{Center} are the x-coordinate, y-coordinate, and z-coordinate of the center of the ellipse primitive modeling, respectively, X_{Major}, Y_{Major}, and Z_{Major} are the components of the major axis direction vector of the ellipse primitive along the x-axis, y-axis, and z-axis, respectively, $iMajorRadius$ is the modeling length of the major axis of the ellipse primitive, $iMinorRadius$ is the modeling length of the minor axis of the ellipse primitive, $iStartParam$ denotes the starting point parameter of the ellipse primitive modeling, $iEndParam$ denotes the ending point parameter of the ellipse primitive modeling, and where $iStartParam$ and $iEndParam$ are within the range of [0, 1].

- Spline primitive

$$SPLINE = \{ID, POINTs\} \tag{6}$$

where *ID* represents the modeling identifier of the spline primitive, and $POINTs$ is the set of point primitives that form the spline primitive.

Before creating the digital model of AFSSRs, the boundary and contour information of the target AFSSR is extracted as a radome wireframe model, taking into consideration the structural form and modeling parameters of the designed AFSSR. The AFSSR's wireframe model is then meticulously dissected in three-dimensional space using basic geometric elements such as point elements, line elements, and curve elements to derive the fundamental element composition of the wireframe model. Subsequently, the contour curves and FSS element of the radome are characterized as diverse primitives, resulting in their respective primitive expressions. Equation (7) represents the general primitive expression of AFSSRs' contour curves, while Equation (8) represents the broad primitive expression of FSS elements.

$$OUTLINE = \{POINT_1, POINT_2, POINT_3, \ldots, POINT_n\} \tag{7}$$

$$UNIT = \{LINEs, CIRCLEs, ELLIPSEs, SPLINEs\} \tag{8}$$

By combining the rules for point primitive, line primitive, and curve primitives described above, the primitive expressions of the rotational airborne radomes' (RARs') generatrix, the shaping lines of duckbill-shaped airborne radomes (DSARs), the contour curves of airborne variable thickness radomes (AVTRs), and the FSS element of AFSSRs are presented. Figure 3 shows the corresponding schematic diagrams, with primitive expressions provided in Equations (9), (10), (12), and (13). By dynamically customizing the primitive of basic geometric elements, refining the expression rules of primitive, establishing standard primitive expressions for commonly used complex geometric shapes, creating PEFs for three-dimensional geometric structures, and adjusting the actual modeling parameters in PEFs, customization and precise modeling of complex spatial structures can be achieved.

$$OUTLINE_{RAR} = SPLINE = \{POINT_1, POINT_2, POINT_3, POINT_4\} \tag{9}$$

$$OUTLINE_{ADSR} = \{LINE_1, LINE_2, LINE_3, LINE_4, CIRCLE_1,\ ELLIPSE_1\} \tag{10}$$

$$Out\ Contour: y = \left(\rho^2 - (x-L)^2 + R - \rho\right)^{\frac{1}{2}},\ \rho = \frac{R^2 + L^2}{2R},\ 0 \le x \le L \tag{11}$$

$$OUTLINE_{AVTR} = \{POINT_1, POINT_2, POINT_3\} \tag{12}$$

$$UNIT = \{LINE_1, LINE_2, LINE_3, \ldots, LINE_8, CIRCLE_1, CIRCLE_2\} \tag{13}$$

3.3. Arrangement Solution for FSS Elements on Undevelopable Surfaces

Currently, the design and analysis of FSSs on airborne radomes under different conditions are predominantly based on ideal plane models or ideal flat plate samples. In the ideal FSS model, the arrangement of FSS elements can be categorized into sparse and dense arrangements based on their density. Among these, sparse arrangements can further be classified into slanted grid arrangments and rectangular grid arrangements according to the angles between the connecting lines of each element center. FSSs designed based on different densities and angles between element center connecting lines often exhibit varying transmission performances [41,42]. However, in practical engineering applications, the aerodynamic shape of AFSSRs is undevelopable in most cases to satisfy the aerodynamic requirements of airborne weapon platforms. AFSSRs designed based on the arrangement of equivalent plane FSS elements may fail to meet the initial EM performance specifications in actual service environments. Therefore, to ensure the satisfactory EM performance of AFSSRs in practical service environments, the arrangement of FSS elements is necessary to be designed according to the aerodynamic shape of the radome. Hereafter, we will discuss the arrangement solutions of FSS elements for rotational radomes and non-rotational radomes, respectively.

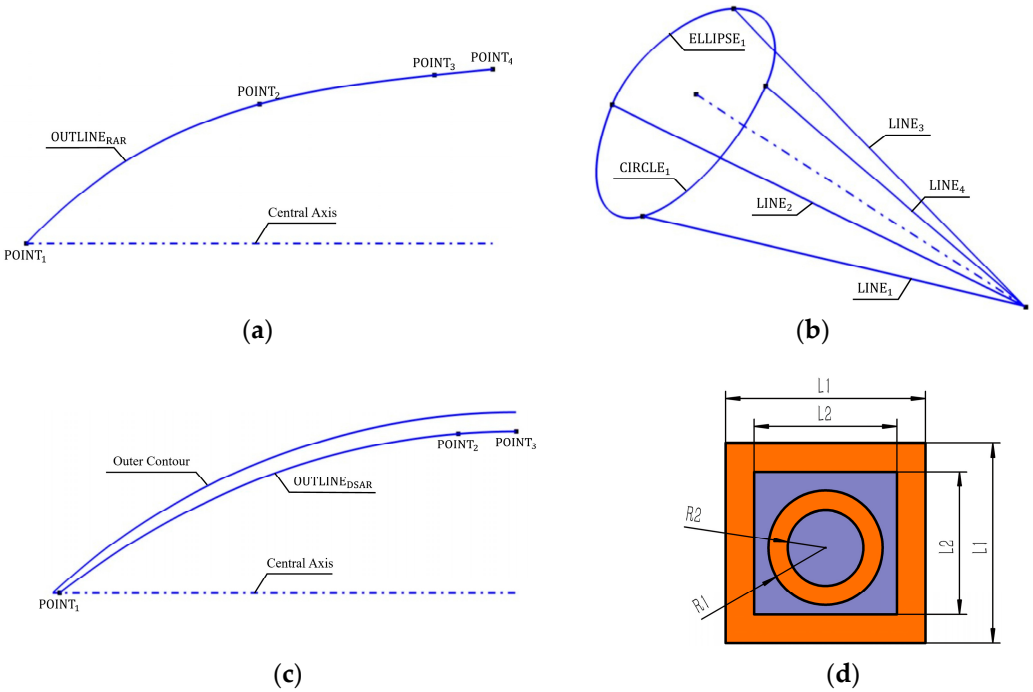


Figure 3. Schematic diagrams of contour curves and an FSS element for various radomes: (**a**) generatrix of rotational airborne radomes; (**b**) shaping lines of duckbill-shaped airborne radomes; (**c**) contour curves of airborne variable thickness radomes; and (**d**) the FSS element.

3.3.1. Arrangement Solution of FSS Elements on Rotational Radomes

1. Arrangement solution of FSS elements along the generatrix

In Figure 4a, curve L_m represents the generatrix of the rotational AFSSR generated by the conical evolution shape Equation (14).

$$y = R\left(\frac{x}{L}\right)^{0.65}, \tag{14}$$

where R is the diameter of the radome, and L is the total length of the radome. Line L_n is the rotational axis of the generatrix, and P_0 and P_3 are two points on L_n. Two auxiliary points, P_1 and P_2, can be determined based on $ApexDistance$ and $TailDistance$, where $ApexDistance$ is the distance from the apexed FSS period to the top of the FSS layer, and $TailDistance$ is the distance from the terminal FSS period to the bottom of the FSS layer. The numerical values of $ApexDistance$ and $TailDistance$ control the specific position of the apexed and terminal FSS periods within the FSS layer of the radome. P_1 and P_2 are projected along the normal from L_n onto L_m to obtain points $P_1^{'}$ and $P_2^{'}$. On undevelopable rotational surfaces such as the FSS of the rotational AFSSR, assuming a spacing D_x between the centers of FSS elements along latitude circles and a spacing of D_y along the generatrix, with a distance $\Delta l_{P_1^{'}P_2^{'}}$ between $P_1^{'}$ and $P_2^{'}$ along L_m, the theoretical number Num_y of FSS periods on the FSS can be determined as

$$Num_y = \frac{\Delta l_{P_1^{'}P_2^{'}}}{D_y} \tag{15}$$

Num_y is also the theoretical number of FSS elements along the generatrix. Let Num_y be an integer value denoted by $Num_y^{'}$, representing the actual number of FSS elements along L_m. Taking $P_1^{'}$ as the reference point for arranging FSS elements along the generatrix, and D_y as the parameter controlling the distance for the arrangement, the center points of each FSS element on L_m can be sequentially determined as N_i, where i belonging to

$\left[1, Num_y^{'}\right]$, and length $\Delta l_{P_1^{'}N_1}$ is equal to $D_y/2$, as illustrated in Figure 4a. Using N_i as the central point allows for the mapping of FSS elements along the L_m.

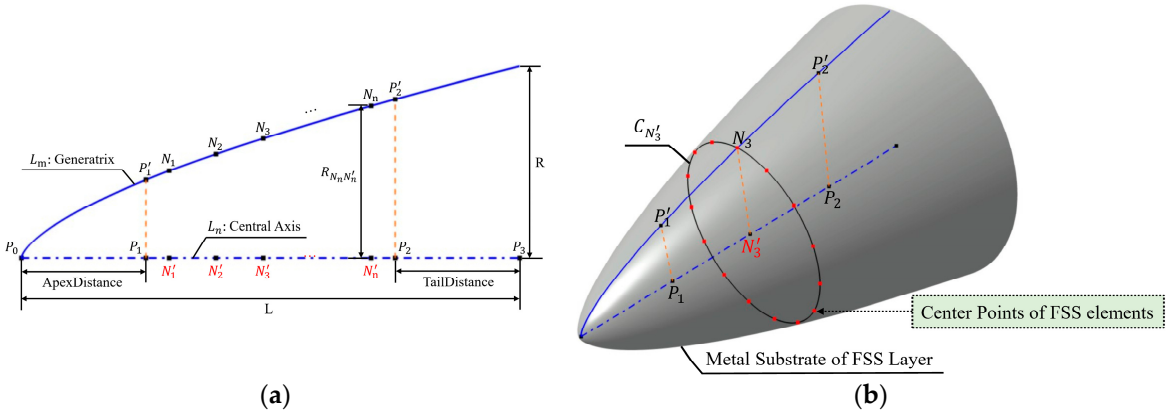


Figure 4. Schematic diagrams of the arrangement solution of FSS elements on rotational radomes: (**a**) arrangement of FSS elements along the generatrix; (**b**) arrangement of FSS elements along latitude circles.

2. Arrangement solution of FSS elements along latitude circles

As shown in Figure 4a, the center points N_i of each FSS element on L_m is projected along the normal direction of L_n to obtain the center $N_i^{'}$ of the latitude circle of the FSS, with i belonging to $\left[1, Num_y^{'}\right]$. The radius corresponding to any latitude circle $C_{N_i^{'}}$ is denoted as $R_{N_iN_i^{'}}$. By considering D_x and $R_{N_iN_i^{'}}$, the theoretical number Num_{x_i} of FSS elements along $C_{N_i^{'}}$ can be determined as

$$Num_{x_i} = \frac{2 \times \pi \times R_{N_iN_i^{'}}}{D_x} \tag{16}$$

Let Num_{x_i} be an integer value denoted by $Num_{x_i}{}^{'}$, and considering $Num_{x_i}{}^{'}$ as the actual number of FSS elements along $C_{N_i^{'}}$, the actual distance $D_{x_i}^{'}$ between the centers of each FSS element along $C_{N_i^{'}}$ is calculated as

$$D_{x_i}^{'} = 2 \times \pi \times \frac{R_{N_iN_i^{'}}}{Num_{x_i}{}^{'}} \tag{17}$$

The average distance error in the arrangement of FSS elements along $C_{N_i^{'}}$, derived from the theoretical spacing D_x along the latitude circle of FSS element centers and the actual spacing $D_{x_i}^{'}$, can be formulated as

$$\Delta D_{x_i} = \left| D_x - D_{x_i}^{'} \right| \tag{18}$$

Taking the center N_3 of the FSS element on the generatrix L_m of the airborne rotational FSS radome as an example, N_3 serves as the reference point for arranging FSS elements along latitude circle $C_{N_3^{'}}$, with $D_{x_3}^{'}$ as the parameter controlling the distance for the arrangement, the center points of the FSS elements along the $C_{N_3^{'}}$ of the FSS can be sequentially determined, as depicted in Figure 4b. As a consequence, this approach allows for the determination of center points for each FSS element on the rotational radome, enabling the arrangement of FSS elements on such undevelopable surfaces of the rotational AFSSR. In the meantime, when customizing the modeling of the generatrix of rotational AFSSRs through the reading of the generatrix's PEF, control over the actual modeling parameters in

the PEF allows the circumference of each FSS period to precisely satisfy integer multiples of the theoretical spacing D_x for centers of FSS elements along latitude circles, thereby minimizing the distance error along latitude circles for each center of FSS elements.

3.3.2. Arrangement Solution of FSS Elements on Non-Rotational Radomes

3. Create a set of isoparametric curves

Figure 5b illustrates a schematic model of the metal FSS layer's substrate created from the PEF based on the shaping lines of the non-rotational AFSSR, where line L_n represents the centerline of the radome, with lines L_{m1} and L_{m2} as well as curves L_{m3} and L_{m4} representing the shaping lines of the radome. L_{m1} and L_{m2} are symmetrical about the L_n. By adjusting the shape of the shaping lines, the aerodynamic shape of the radome can be altered. On undevelopable non-rotational surfaces such as the FSS of non-rotational AFSSRs, isoparametric curves parallel to L_{m3} and L_{m4} can be constructed on the surface of the radome as auxiliary lines for the arrangement of FSS elements. Isoparametric curves are a graphical representation of a dependent variable within a system where all parameters remain constant and the curve varies only with the independent variable. In the digital modeling process of the non-rotational AFSSR, a set of isoparametric curves can be constructed by using the starting positions of FSS periods determined on L_{m1} or L_{m2} as the independent variable, with the starting positions of FSS periods and the tangential direction of the radome's outer surface in each frequency selection cycle as constant parameters.

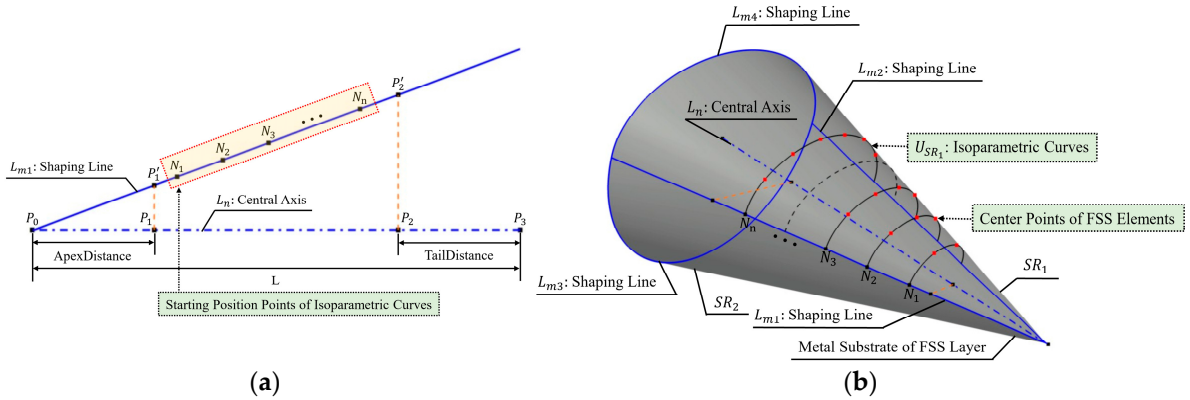


Figure 5. Schematic diagrams of the arrangement solution of FSS elements on non-rotational radomes: (**a**) schematic diagram of starting position points of isoparametric curves; (**b**) arrangement of FSS elements along isoparametric curves.

Here, taking L_{m1} as an example to determine the starting positions of FSS periods, further elaboration is as follows on the arrangement solution of FSS elements on the non-rotational AFSSR: The plane in which Figure 5a is located is determined by L_{m1} and L_n, where points P_0 and P_3 lie on L_n, and length $\Delta l_{P_0P_3}$ represents the total length L of the radome. Two auxiliary points, P_1 and P_2, can be determined based on $ApexDistance$ and $TailDistance$, where $ApexDistance$ is the distance from the apexed FSS period to the top of the FSS layer, and $TailDistance$ is the distance from the terminal FSS period to the bottom of the FSS layer. The projection of P_1 and P_2 along the normal direction to L_n onto the L_{m1} results in points $P_1^{'}$ and $P_2^{'}$. On undevelopable non-rotational surfaces such as the FSS of the non-rotational AFSSR, assuming the spacing between the centers of FSS elements along isoparametric curves is D_x and the spacing along shaping lines L_{m1} or L_{m2} is D_y, and the spacing between P_1 and P_2 along L_n is a distance $\Delta l_{P_1'P_2'}$, the theoretical number Num_y of FSS periods for the FSS can be obtained from D_y and $\Delta l_{P_1'P_2'}$ as follows:

$$Num_y = \frac{\Delta l_{P_1'P_2'}}{D_y} \tag{19}$$

Let Num_y be an integer value denoted by $Num_y^{'}$, with $Num_y^{'}$ representing the actual number of FSS periods for the radome. Taking $P_1^{'}$ as the reference point for the starting position of FSS periods and D_y as the parameter controlling the distance for each FSS period, the starting position point N_i for each FSS period can be sequentially determined on L_{m1}, where i belongs to $\left[1, Num_y^{'}\right]$ and length $\Delta l_{P_1^{'}N_1}$ is equal to $D_y/2$, as shown in Figure 5a. By considering N_i as the independent variable for each isoparametric curve and the upper surface SR_1 of the radome along with its tangential direction at N_i as constant parameters, a set U_{SR_1} of isoparametric curves can be constructed on SR_1, as illustrated in Figure 5b.

4. Arrangement solution of FSS elements along isoparametric curves

Assuming the isoparametric curve determined by N_i is denoted as I_{N_i}, with the length of the I_{N_i} being l_i, the theoretical number of FSS elements along Ii can be obtained from D_x and l_i as follows:

$$Num_{x_i} = \frac{l_i}{D_x} \tag{20}$$

Let Num_{x_i} be an integer value denoted by $Num_{x_i}{}^{'}$, representing the actual number of FSS elements along I_{N_i}. The actual distance between the centers of each FSS element along the I_{N_i} is calculated as

$$D_{x_i}^{'} = \frac{l_i}{Num_{x_i}{}^{'}} \tag{21}$$

The average distance error in the arrangement of FSS elements along isoparametric curve I_{N_i}, based on the theoretical spacing D_x and the actual spacing $D_{x_i}^{'}$ along the I_{N_i}, can be formulated as

$$\Delta D_{x_i} = \left| D_x - D_{x_i}^{'} \right| \tag{22}$$

Using the N_i of each FSS period on the L_{m1} of the radome as the reference points for arranging FSS elements along the corresponding isoparametric curves Ii, with $D_{x_i}^{'}$ as the parameter controlling the distance for the arrangement, the center points of the FSS elements along the I_{N_i} on the surface of the FSS layer can be sequentially determined, as shown in Figure 5b. As a result, this approach can determine the center points for FSS elements of each FSS period on the non-rotational radome for the arrangement of FSS elements on such undevelopable surfaces of the non-rotational AFSSR. Moreover, when modeling the shaping lines of non-rotational AFSSRs based on the PEFs of the shaping lines, the curvature of the upper and lower surfaces can be controlled by the shaping line, ensuring that the lengths of each isoparametric curve are exactly integer multiples of theoretical spacing D_x for the center of FSS elements, thereby reducing the distance error of the center of each FSS element along the corresponding isoparameter curve.

3.4. Mapping Method for FSS Elements

Based on the above-mentioned arrangement solution of FSS elements on undevelopable surfaces, the center points of each FSS element on the metal substrate's surface of the FSS layer can be determined. The process of mapping planar elements into curved surface elements is described below, as shown in Figure 6. Firstly, a tangent plane is passed through the center point of any FSS element on the surface of the metal substrate of the FSS layer. Then, the planar model of the FSS element is carried out on the tangent plane. Finally, mapping the planar element onto the metal substrate of the FSS layer generates the FSS element on the undevelopable surface.

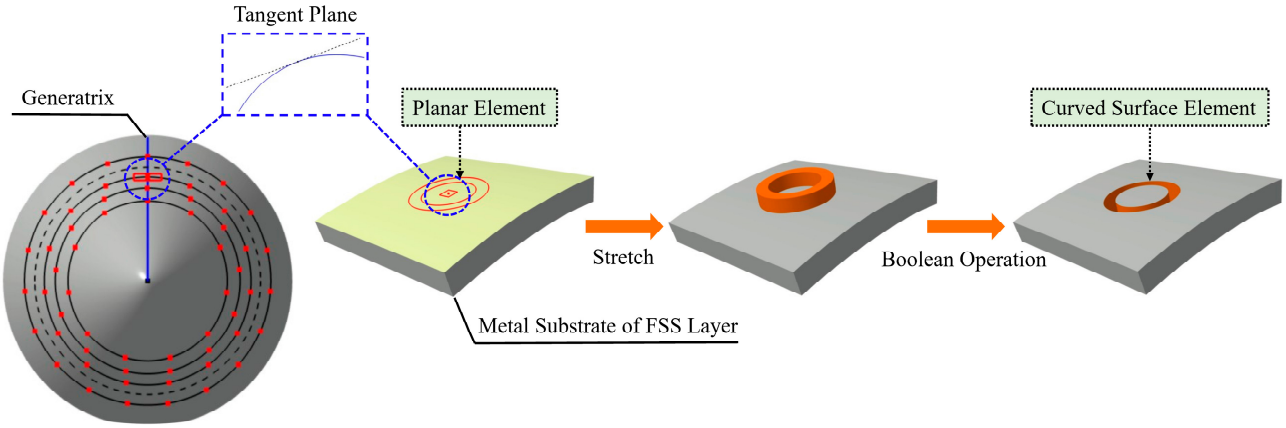


Figure 6. Schematic diagram of mapping planar elements into curved surface elements.

3.5. Implementation of the Sub-Model and the Whole Machine Model

The logical implementation of this method is based on commercial CAD software's APIs, incorporating expression rules of primitives, arrangement solutions and mapping methods for FSS elements on undevelopable surfaces, manual modeling methods, manual modeling knowledge encapsulation into the modeling functions of the dielectric layers and FSS layers, and assembly functions of the whole machine model. After determining the layered scheme for the digital model of AFSSRs, the modeling functions of the dielectric layers and the FSS layers are called separately to create models of dielectric layers and FSS layers. The assembly function of the whole machine model is then used to assemble each layer according to their inter-layer relationships, ultimately generating the whole machine model of the AFSSR. With this step, the digital modeling of the AFSSR is completed. Figures 7 and 8 show the modeling algorithm flowchart for the sub-models and the assembly algorithm flowchart for the whole machine model, respectively.

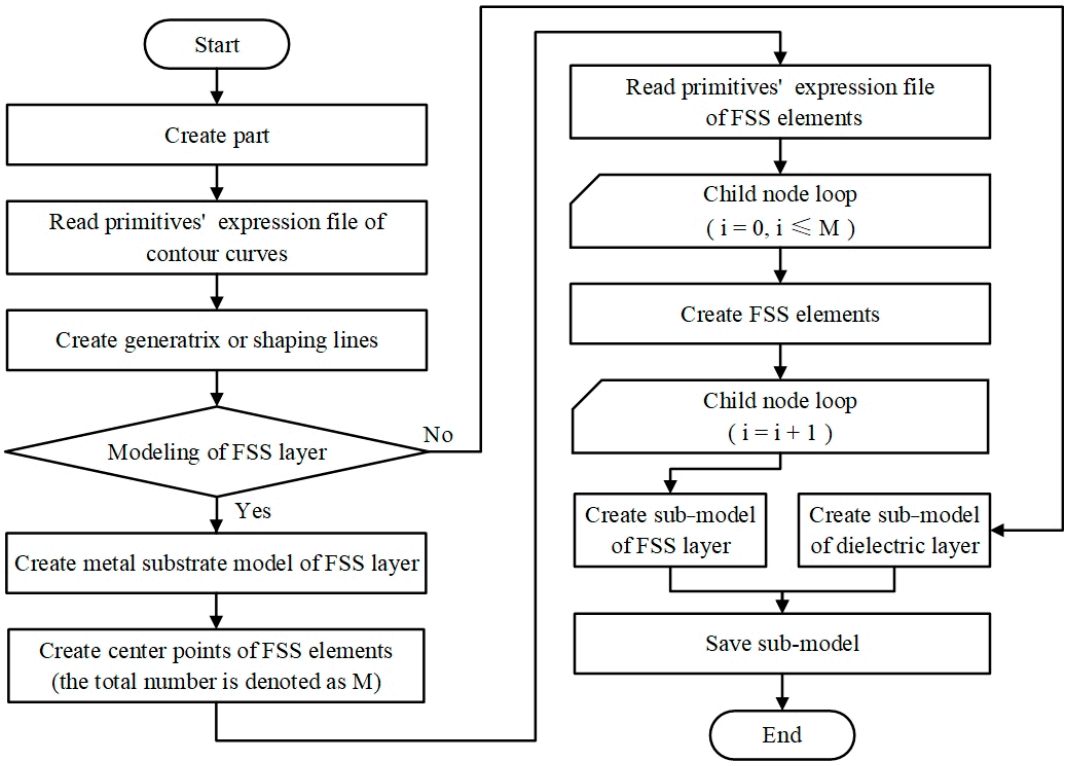


Figure 7. Modeling algorithm flowchart for the sub-models.

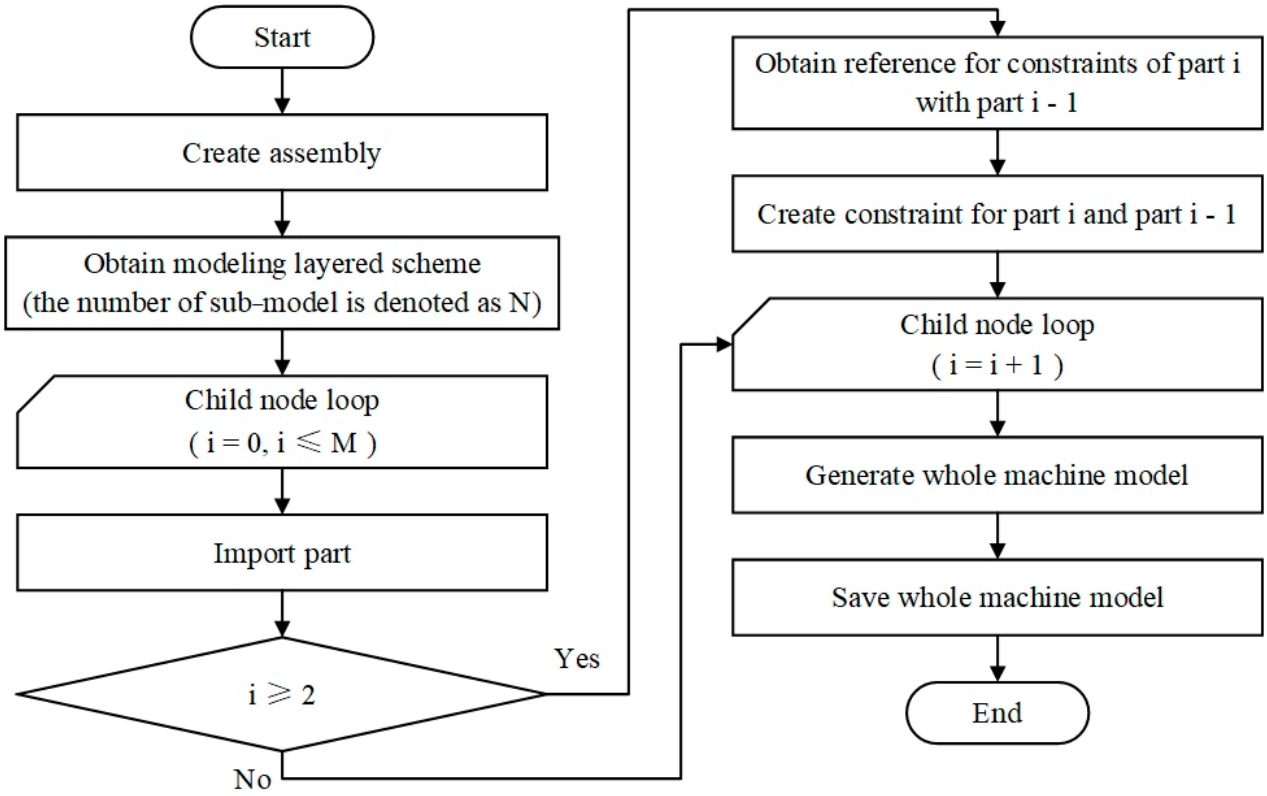


Figure 8. Assembly algorithm flowchart for the whole machine model.

4. System Construction and Example Verification

4.1. Construction of a Rapid Modeling System

Based on the rapid modeling solution for AFSSRs described above, this section utilizes CATIA software as the modeling tool and combines it with the CATIA API, rules for primitive expression, arrangement solution, and mapping method for FSS elements on undevelopable surfaces, manual modeling methods, and manual modeling knowledge to establish a system for the rapid modeling of AFSSRs. As shown in Figure 9, the system's interactive interface includes an input area on the left for the structural form and modeling parameters of the target AFSSR and a modeling process display area for the modeling tool on the right. The rapid modeling of the target AFSSR using this system is divided into the following three phases:

5. Modeling preparation phase.

Structural designers pre-determine the structural form and modeling parameters of the target AFSSR and construct PEFs of contour curves and FSS elements.

6. Human–computer interaction phase.

Structural designers open the system, select the desired structural form of the radome body, input modeling parameters, and import the PEFs built in the first phase into the interactive interface of the system. Then, they need to use the system to check whether the structural forms and modeling parameters meet the geometric conditions of the digital model of the target AFSSR. If satisfied, the modeling button is activated, leading to the third phase. If not satisfied, the structural form and modeling parameters of the target AFSSR need to be adjusted.

7. Modeling phase.

Clicking the modeling button activated in the second phase will call the modeling tool to automatically create the digital model of the target AFSSR in the modeling process display area.

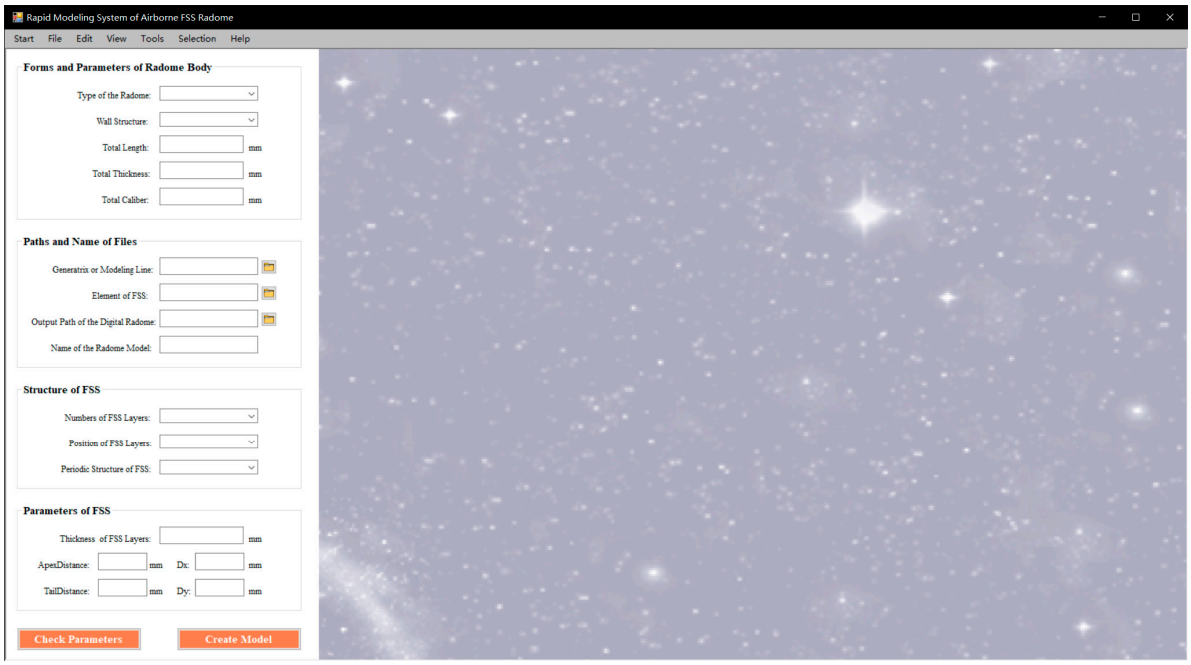


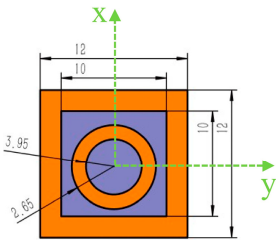
Figure 9. Schematic diagram of the system's interactive interface.

4.2. Demonstration of the Rapid Modeling Effect

Taking the modeling of a rotational AFSSR with an A-sandwich wall structure and dual-screen FSS as an example, the modeling effect of the system is demonstrated. The structural form and modeling parameters of the radome are exhibited in Table 1, and Figure 10a displays a schematic diagram of the FSS element of the radome. The content of the PEF for the FSS element is shown in Figure 10b.

Table 1. Modeling parameters of the rotational airborne frequency selective surface radome (AFSSR) with an A-sandwich wall structure and dual-screen frequency selective surface (FSS).

Parameter	Value	Parameter	Value
structural form	rotational	*ApexDistance*	150 mm
wall structure	A-sandwich	*TailDistance*	50 mm
total length	800 mm	numbers of FSS layers	two-layer
total thickness	12 mm	position of FSS layers	skin-core junction
total caliber	400 mm	periodic structure of FSS	aperture
thickness of FSS layers	2 mm	D_x	12 mm
thickness of skin layers	2 mm	D_y	12 mm
thickness of inter layer	4 mm	numbers of FSS elements	8589



(**a**)

ID: LINE	X–Start	Y–Start	Z–Start	X–End	Y–End	Z–End
ID: CIRCLE	X–Center	Y–Center	Z–Center	iRadius	iStartRaram	iEndParam
CIRCLE	0	0	0	3.95	0	1
CIRCLE	0	0	0	2.65	0	1
LINE	-5	5	0	5	5	0
LINE	5	5	0	5	-5	0
LINE	5	-5	0	-5	-5	0
LINE	-5	-5	0	-5	5	0

(**b**)

Figure 10. A schematic diagram of the FSS element and its PEF: (**a**) FSS element; (**b**) content of the PEF.

Running the system on a computer configured with an Intel i5-13600KF processor and 32 GB of memory, the data from Table 1 are input into the system's interactive interface, and the PEF is imported into the system. The exploded view of the digital model of the target AFSSR obtained is shown in Figure 11a. Figure 11b displays one of the dual-screen FSS models of the digital model, while Figure 11c illustrates the wall structural diagram of the target AFSSR. The total number of elements in the dual-screen FSS is 8589, and the modeling process took 14 min and 23 s.

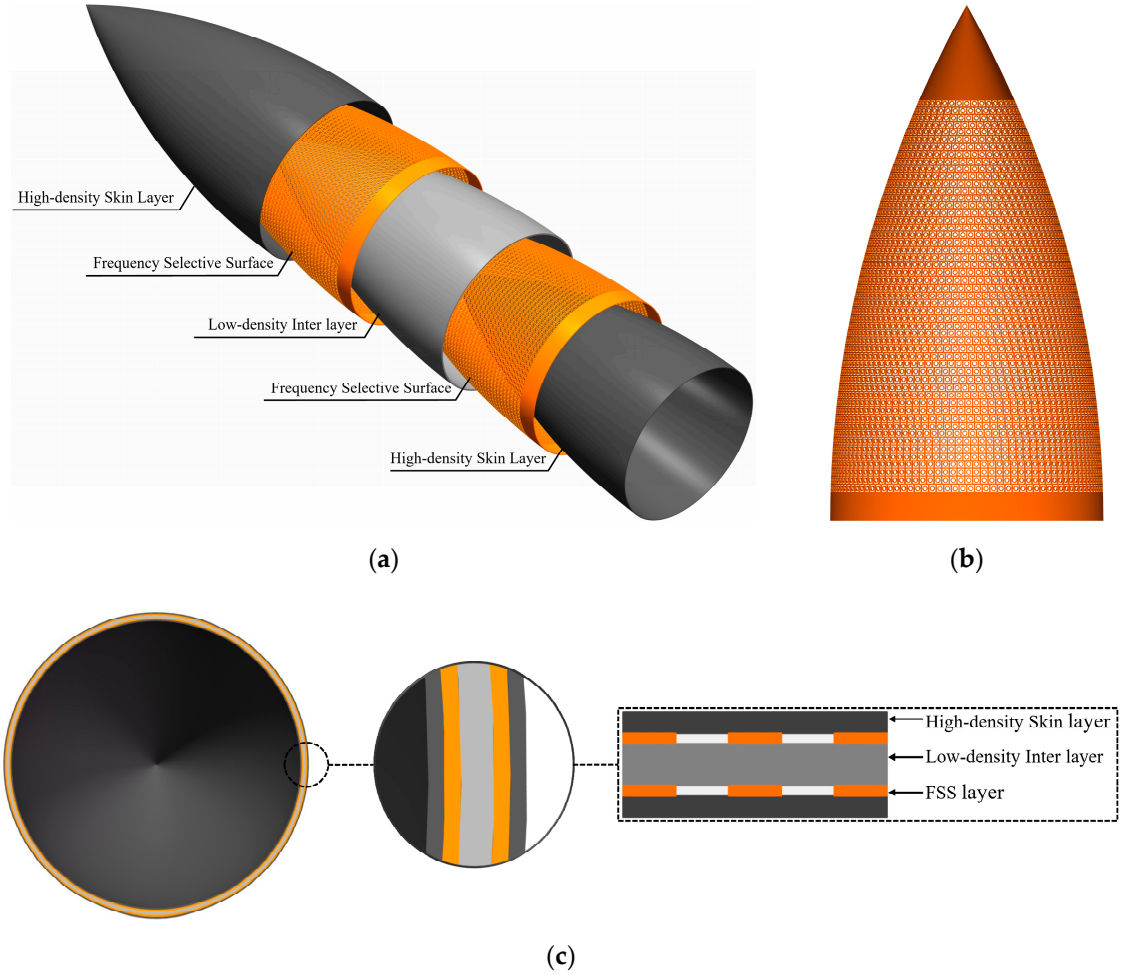


Figure 11. Digital model of the rotational AFSSR with an A-sandwich wall structure and dual-screen FSS (**a**) Exploded view; (**b**) One of the dual-screen FSS models. (**c**) AFSSR wall structure.

4.3. Comparison of Rapid Modeling Efficiency

The efficiency of different modeling methods is compared by creating models with three different structural forms, labeled as models A, B, and C. The structural forms and modeling parameters of models A, B, and C are shown in Tables 1–3, respectively, with schematic diagrams depicted in Figures 11–13. Three models were created using manual modeling methods, the HFSS-MATLAB combined modeling method and the method described in this paper, respectively. The time consumed for each model creation is presented in Table 4. Compared with the manual modeling methods and the MATLAB-HFSS combined modeling method, this method saves at least 95% and 91.6% of the time for creating model A, at least 95.5% and 80% of the time for creating model B, and at least 97.5% and 85% of the time for creating model C. The research results indicate that, compared to conventional modeling methods, the method proposed in this study significantly reduces modeling time and enhances modeling efficiency.

Table 2. Modeling parameters for Model B.

Parameter	Value	Parameter	Value
structural form	non-rotational	$ApexDistance$	100 mm
wall structure	solid-core	$TailDistance$	50 mm
total length	400 mm	periodic structure of FSS	patch
total thickness	6 mm	type of FSS elements	ring-shaped
total caliber	250 mm	size of FSS elements	R6.5 mm × R4 mm
thickness of FSS layers	2 mm	D_x	15 mm
numbers of FSS layers	one-layer	D_y	15 mm
position of FSS layers	middle	numbers of FSS elements	530

Table 3. Modeling parameters for Model C.

Parameter	Value	Parameter	Value
structural form	rotational	$ApexDistance$	100 mm
wall structure	solid-core	$TailDistance$	50 mm
total length	600 mm	periodic structure of FSS	aperture
total thickness	6 mm	type of FSS elements	Y-ring-shaped
total caliber	300 mm	size of FSS elements	L6 mm × W4 mm × B1 mm × A60°
thickness of FSS layers	2 mm	D_x	15 mm
numbers of FSS layers	one-layer	D_y	14 mm
position of FSS layers	middle	numbers of FSS elements	1582

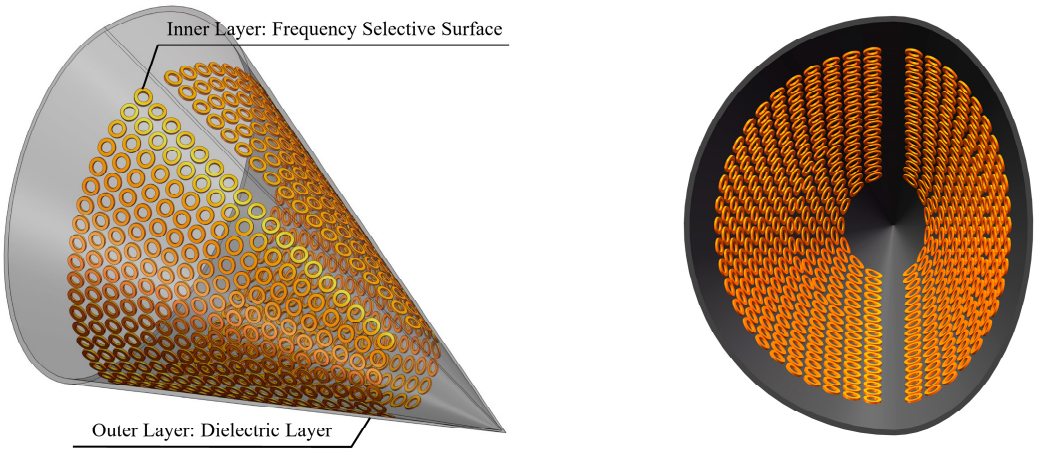


Figure 12. Schematic diagram of the model B: (**a**) schematic diagram of the whole machine model; (**b**) schematic of the interior of the radome.

Table 4. Time required to build models A, B, and C by different methods.

	Manual Methods	HFSS-MATLAB Combined Method	Method Described in This Paper
Model A	≥300 min	≥180 min	≤15 min
Model B	≥180 min	≥40 min	≤8 min
Model C	≥120 min	≥20 min	≤3 min

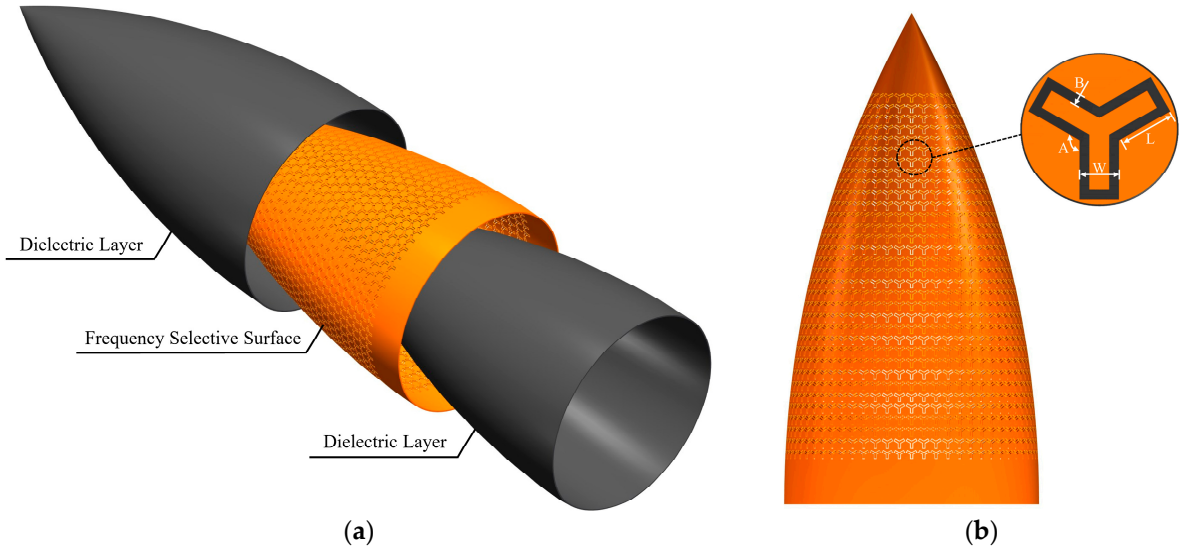


Figure 13. Schematic diagram of the model C: (**a**) exploded view; (**b**) FSS layer.

Based on the research results of this section, it is evident that the rapid modeling method for AFFRs based on dynamic customizable primitives proposed in this paper not only achieves customization and precision of the radome model by defining expression rules of primitives and creating PEFs to represent contour curves and FSS elements of the target radome, but also realizes the automation and rapidity of the radome modeling process by constructing modeling functions and setting up modeling systems.

5. Conclusions

This paper presents a rapid modeling method for AFFRs based on dynamic customizable primitives. This method relies on PEFs as underlying support to achieve customization and precision in the digital modeling of AFSSRs, and modeling functions for the dielectric layers, FSS layer, and whole machine serve as the logical implementation to automate and accelerate the modeling process. Subsequently, the construction of a rapid modeling system based on this method has demonstrated the following results through practical applications: Firstly, the representation of radome boundaries and contours is flexible and accurate through primitives. Secondly, the modeling process is autonomously completed by commercial CAD software. Lastly, compared to conventional modeling methods, a significant reduction in modeling time and enhanced efficiency are observed (with efficiency improvement ranging from approximately 20% to 97.5%, with efficiency increasing with the number of FSS elements). Future efforts will focus on refining the types and representation rules of primitives, expanding the arrangement solution of FSS elements, optimizing modeling procedures and systems, and broadening the application of this method in the field of AFSSRs.

Author Contributions: Conceptualization, C.Q. and S.L.; methodology, C.Q.; software, C.Q.; validation, C.Q., X.L. and Z.Y.; formal analysis, Y.C.; investigation, S.S.; resources, L.S.; data curation, S.L.; writing—original draft preparation, C.Q.; writing—review and editing, C.Q.; visualization, C.Q.; supervision, W.Z.; project administration, S.L.; funding acquisition, L.S. All authors have read and agreed to the published version of the manuscript.

Funding: This research was funded by the National Natural Science Foundation of China under Grant U2241205.

Institutional Review Board Statement: Not applicable.

Informed Consent Statement: Not applicable.

Data Availability Statement: Data are contained within the article.

Acknowledgments: The author would like to thank the editor-in-chief, associate editors, and reviewers for their valuable comments and suggestions.

Conflicts of Interest: The authors declare no conflicts of interest.

References

1. Li, P.; Pedrycz, W.; Xu, W.; Song, L. Far-Field Pattern Tolerance Analysis of the Antenna-Radome System With the Material Thickness Error: An Interval Arithmetic Approach. *IEEE Trans. Antennas Propag.* **2017**, *65*, 1934–1946. [CrossRef]
2. Wei, Z.; Zhou, C.; Zhang, F.; Zhou, C. Reliability Optimization of the Honeycomb Sandwich Structure Based on A Neural Network Surrogate Model. *Materials* **2023**, *16*, 7465. [CrossRef]
3. Kandi, K.K.; Thallapalli, N.; Chilakalapalli, S.P.R. Development of Silicon Nitride-Based Ceramic Radomes—A Review. *Int. J. Appl. Ceram. Technol.* **2014**, *12*, 909–920. [CrossRef]
4. Kenion, T.; Yang, N.; Xu, C. Dielectric and mechanical properties of hypersonic radome materials and metamaterial design: A review. *J. Eur. Ceram. Soc.* **2022**, *42*, 1–17. [CrossRef]
5. Kim, P.C.; Lee, D.G. Composite sandwich constructions for absorbing the electromagnetic waves. *Compos. Struct.* **2009**, *87*, 161–167. [CrossRef]
6. Son, D.-S.; Hyun, J.-M.; Chaki, S.; Park, C.H.; Lee, J.-R. Evaluation of Mechanical/Electromagnetic Preformation of Single-Sided Active Frequency Selective Surface for Stealth Radomes. *Int. J. Aeronaut. Space Sci.* **2021**, *22*, 1235–1242. [CrossRef]
7. Kim, P.; Lee, D.; Seo, I.; Kim, G. Low-observable radomes composed of composite sandwich constructions and frequency selective surfaces. *Compos. Sci. Technol.* **2008**, *68*, 2163–2170. [CrossRef]
8. Wu, K.; Xu, W.; Li, P.; Zhou, J.; Li, W. Miniaturised element frequency selective surface design for high power microwave applications. *IET Microw. Antennas Propag.* **2023**, *17*, 846–856. [CrossRef]
9. Panwar, R.; Lee, J.R. Progress in frequency selective surface-based smart electromagnetic structures: A critical review. *Aerosp. Sci. Technol.* **2017**, *66*, 216–234. [CrossRef]
10. Narayan, S.; Jha, R.M. Electromagnetic Techniques and Design Strategies for FSS Structure Applications [Antenna Applications Corner]. *IEEE Antennas Propag. Mag.* **2015**, *57*, 135–158. [CrossRef]
11. Anwar, R.; Mao, L.; Ning, H. Frequency Selective Surfaces: A Review. *Appl. Sci.* **2018**, *8*, 1689. [CrossRef]
12. Choi, I.; Lee, D.; Lee, D.G. Hybrid composite low-observable radome composed of E-glass/aramid/epoxy composite sandwich construction and frequency selective surface. *Compos. Struct.* **2014**, *117*, 98–104. [CrossRef]
13. Narayan, S.; Gulati, G.; Sangeetha, B.; Nair, R.U. Novel Metamaterial-Element-Based FSS for Airborne Radome Applications. *IEEE Trans. Antennas Propag.* **2018**, *66*, 4695–4707. [CrossRef]
14. Liu, N.; Sheng, X.; Zhang, C.; Fan, J.; Guo, D. Design of FSS radome using binary particle swarm algorithm combined with pixel-overlap technique. *J. Electromagn. Waves Appl.* **2017**, *31*, 522–531. [CrossRef]
15. Rafieipour, H.; Setoodeh, A.; Kin-Tak Lau, A. Mechanical and electromagnetic behavior of fabricated hybrid composite sandwich radome with a new optimized frequency-selective surface. *Compos. Struct.* **2021**, *273*, 114256. [CrossRef]
16. Xu, W.; Duan, B.Y.; Li, P.; Qiu, Y. Study on the Electromagnetic Performance of Inhomogeneous Radomes for Airborne Applications—Part I: Characteristics of Phase Distortion and Boresight Error. *IEEE Trans. Antennas Propag.* **2017**, *65*, 3162–3174. [CrossRef]
17. Nair, R.U.; Jha, R.M. Electromagnetic Design and Performance Analysis of Airborne Radomes: Trends and Perspectives. *IEEE Antennas Propag. Mag.* **2014**, *56*, 276–298. [CrossRef]
18. Wang, Z.; Tang, L.; Zhou, L.; Jiang, Z.; Liu, Z.; Liu, Y. Methodology to Design Variable-Thickness Streamlined Radomes With Graded Dielectric Multilayered Wall. *IEEE Trans. Antennas Propag.* **2021**, *69*, 8015–8020. [CrossRef]
19. Vinisha, C.V.; Mohammed Yazeen, P.S.; Mahima, P.; Joy, V.; Nair, R.U. Multi-layered graded porous radome design for dual-band airborne radar applications. *Electron. Lett.* **2017**, *53*, 189–191. [CrossRef]
20. Xu, W.; Zong, Y.; Li, P.; Qiu, Y. Variable Thickness Airborne Radome Design Considering Thickness Profile Control and Additional Electromagnetic Performance. *IEEE Trans. Antennas Propag.* **2021**, *69*, 2443–2448. [CrossRef]
21. Xu, W.; Duan, B.Y.; Li, P.; Qiu, Y. A New Efficient Thickness Profile Design Method for Streamlined Airborne Radomes. *IEEE Trans. Antennas Propag.* **2017**, *65*, 6190–6195. [CrossRef]
22. Xu, W.; Duan, B.Y.; Li, P.; Qiu, Y. Study on the Electromagnetic Performance of Inhomogeneous Radomes for Airborne Applications—Part II: The Overall Comparison With Variable Thickness Radomes. *IEEE Trans. Antennas Propag.* **2017**, *65*, 3175–3183. [CrossRef]
23. de Lucena Nóbrega, C.; Ribeiro da Silva, M.; da Fonseca Silva, P.H.; D'Assunção, A.G. A compact frequency selective surface with angular stability based on the Sierpinski fractal geometry. *J. Electromagn. Waves Appl.* **2013**, *27*, 2308–2316. [CrossRef]
24. Murugasamy, L.; Sivasamy, R. A Novel Fractal Inspired Iterated Four-Legged Loaded Loop Elements Based 2.5-D Miniaturized Frequency Selective Surface. *IEEE Trans. Electromagn. Compat.* **2021**, *63*, 2164–2167. [CrossRef]
25. Yang, Z.; Luo, F.; Zhou, W.; Jia, H.; Zhu, D. Design of a thin and broadband microwave absorber using double layer frequency selective surface. *J. Alloys Compd.* **2017**, *699*, 534–539. [CrossRef]
26. Solunke, Y.; Kothari, A. An ultra-thin, low-RCS, dual-bandpass novel fractal-FSS for planar/conformal C&X bands applications. *AEU-Int. J. Electron. Commun.* **2024**, *175*, 155073. [CrossRef]

27. Sheng, X.; Wang, H.; Liu, N.; Wang, K. A Conformal Miniaturized Bandpass Frequency-Selective Surface With Stable Frequency Response for Radome Applications. *IEEE Trans. Antennas Propag.* **2024**, *72*, 2423–2433. [CrossRef]
28. Grendysa, W.; Joël, J.; Emmanuel, B. Parametric model of aircraft external geometry as a component of FAST-OAD aircraft preliminary design system. *J. Phys. Conf. Ser.* **2023**, *2526*, 012030. [CrossRef]
29. Ma, L.; Zhang, Q.J.; Liu, W.; Zhang, J. Advances in hybrid format-based neuro-transfer function techniques for parametric modeling of microwave components. *Int. J. Numer. Model. Electron. Netw. Devices Fields* **2023**, *37*, e3122. [CrossRef]
30. Chen, L.; Zhang, L.; Wu, Y.; Xu, G.; Li, B. Isogeometric Size Optimization Design Based on Parameterized Volume Parametric Models. *Comput. Aided Des.* **2024**, *169*, 103672. [CrossRef]
31. Zheng, L.; Chen, S.; Ji, S.; Chen, Z. An improved parametric model for marine propeller: iPM4MP. *Ocean Eng.* **2023**, *287*, 115712. [CrossRef]
32. Tang, Z.; Zou, Q.; Gao, S. A decision-support method for multi-parameter editing of parametric CAD models. *Adv. Eng. Inform.* **2023**, *56*, 101997. [CrossRef]
33. Saeedi Heydari, M.; Ghezavati, J.; Abbasgholipour, M.; Mohammadi Alasti, B. Various types of ceramics used in radome: A review. *Sci. Iran.* **2017**, *24*, 1136–1147. [CrossRef]
34. Wang, Q.; Li, P.; Rocca, P.; Li, R.; Tan, G.; Hu, N.; Xu, W. Interval-Based Tolerance Analysis Method for Petal Reflector Antenna With Random Surface and Deployment Errors. *IEEE Trans. Antennas Propag.* **2023**, *71*, 8556–8569. [CrossRef]
35. Ding, G.; Anselmi, N.; Xu, W.; Li, P.; Rocca, P. Interval-Bounded Optimal Power Pattern Synthesis of Array Antenna Excitations Robust to Mutual Coupling. *IEEE Antennas Wirel. Propag. Lett.* **2023**, *22*, 2725–2729. [CrossRef]
36. Nag, A.; Rao, R.R.; Panda, P.K. High temperature ceramic radomes (HTCR)—A review. *Ceram. Int.* **2021**, *47*, 20793–20806. [CrossRef]
37. Yang, J.; Zheng, H.; Pang, Y.; Qu, B.; Li, Y.; Wang, J.; Xu, Z. Design, modelling, and manufacturing of sandwich radome structure with out-of-band absorption and in-band transmission performances. *Compos. Struct.* **2024**, *339*, 118138. [CrossRef]
38. Chen, X.Y.; Feng, Y.W.; Song, Z.C.; Zhou, C.P. Mechanical property analysis and experimental validation of composite honeycomb sandwich radome considering perforation and impact damage. *Conf. Ser.* **2024**, *2746*, 012048. [CrossRef]
39. Hao, L.; Gang, Q.; Wang, X.; Wang, K.; Zheng, Y. Study on Shear Fatigue Performance of Scarf Repaired Honeycomb Sandwich Structure. *J. Phys. Conf. Ser.* **2024**, *2671*, 012014. [CrossRef]
40. Zhou, L.; Wang, P.; Pei, Y.; Zeng, A.; Tang, L.; Liu, Z.; Liu, Y.; Jiang, Z.; Fang, D. Design and characterization for dual-band and multi-band A-sandwich composite radome walls. *Compos. Sci. Technol.* **2017**, *149*, 28–33. [CrossRef]
41. Jin, L.; Zhao, Y.; Chen, C.; Zhang, J.; He, Y.; Yin, C.; Wu, N.; Tang, J.; Xing, S. Application, development, and challenges of stealth materials/structures in next-generation aviation equipment. *Appl. Surf. Sci. Adv.* **2024**, *19*, 100575. [CrossRef]
42. Venkatesh, G.; Singh, S.P.; Thottappan, M. A novel fast roll-off bandpass frequency selective surface for stealth applications. *J. Electromagn. Waves Appl.* **2024**, *38*, 571–581. [CrossRef]

Disclaimer/Publisher's Note: The statements, opinions and data contained in all publications are solely those of the individual author(s) and contributor(s) and not of MDPI and/or the editor(s). MDPI and/or the editor(s) disclaim responsibility for any injury to people or property resulting from any ideas, methods, instructions or products referred to in the content.